Supplemental Figures

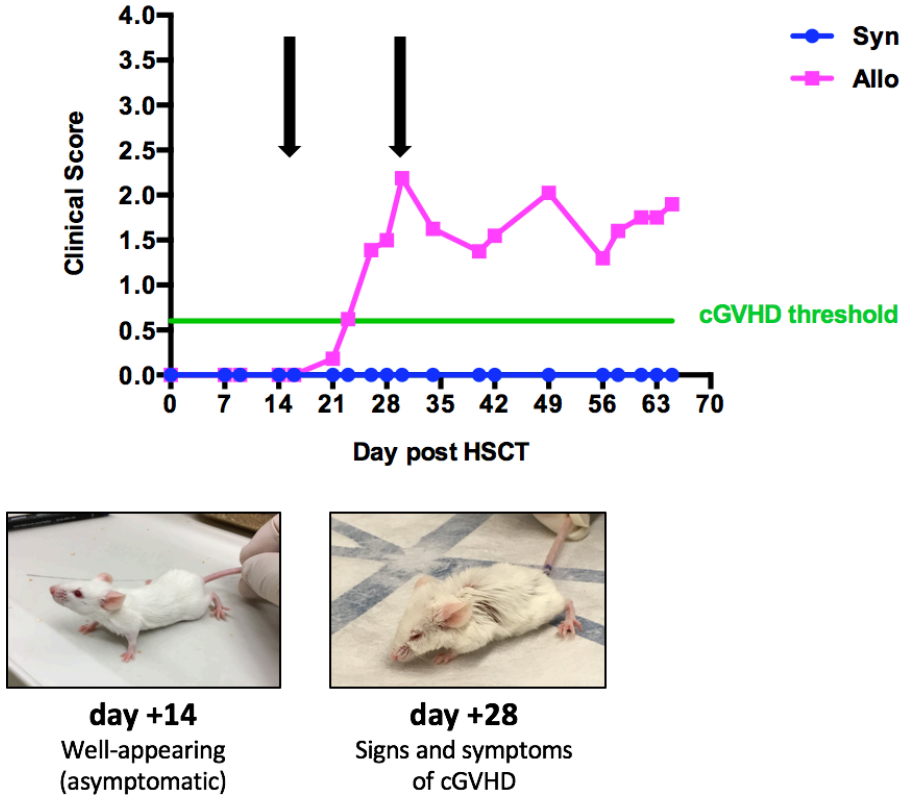

Supplemental Figure 1. Clinical scoring data for mice undergoing hematopoietic stem cell transplantation (HSCT). Typical clinical score curve for mice in syngeneic and allogeneic cohorts at specified post HSCT time points. Green line represents a clinical score of 0.6, minimum score for considering mice as having clinical evidence of chronic graft-vs-host disease (cGVHD). Data for day 0 through +35 are representative of more than ten independent experiments.

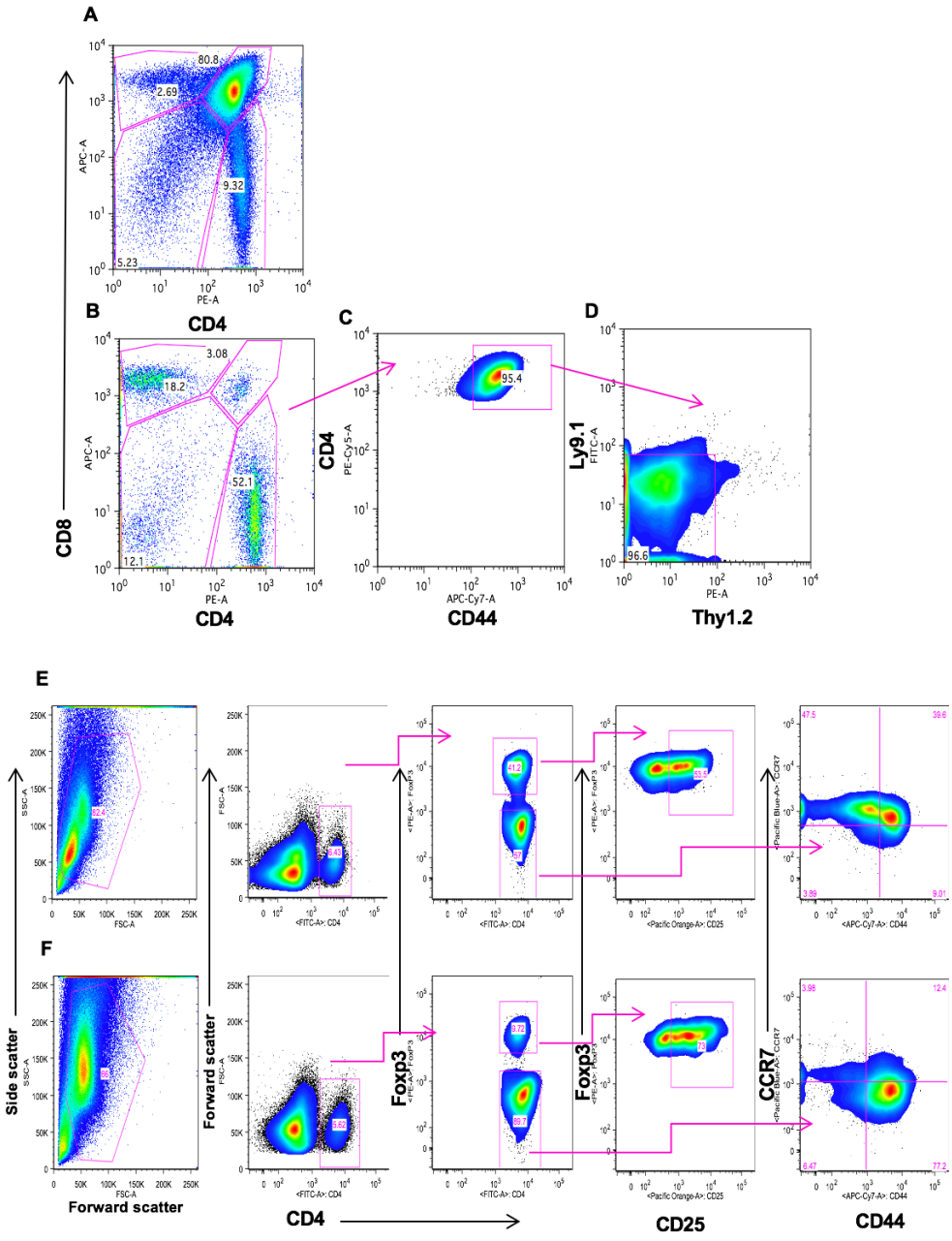

Supplemental Figure 2. Lymphoid immune reconstitution in allogeneic recipients is characterized by donor peripherally-expanded mature CD4+ T cell predominance. Thymic immune-reconstitution following hematopoietic stem cell transplantation evaluated by flow cytometry at day +30. **(A)** Syngeneic recipients show a predominance of double positive thymocytes ($CD4^+$ $CD8^+$). **(B)** Allogeneic recipients show a predominance of single positive $CD4^+$, and near absence of double positive and double negative thymocytes ($CD4^-CD8^-$). **(C)** These single positive $CD4^+$ cells are primarily of memory ($CD44^+$) phenotype. **(D)** Congenic markers showed that $CD4^+CD44^+$ cells were of donor-derived peripherally expanded phenotype ($Ly9.1^-Thy1.2^-$). Data are representative of three independent experiments (**A** and **B**) and two independent experiments (**C** and **D**). Flow cytometry gating strategy for spleen samples, with **(E)** syngeneic and **(F)** allogeneic cohort representative data for day +14.

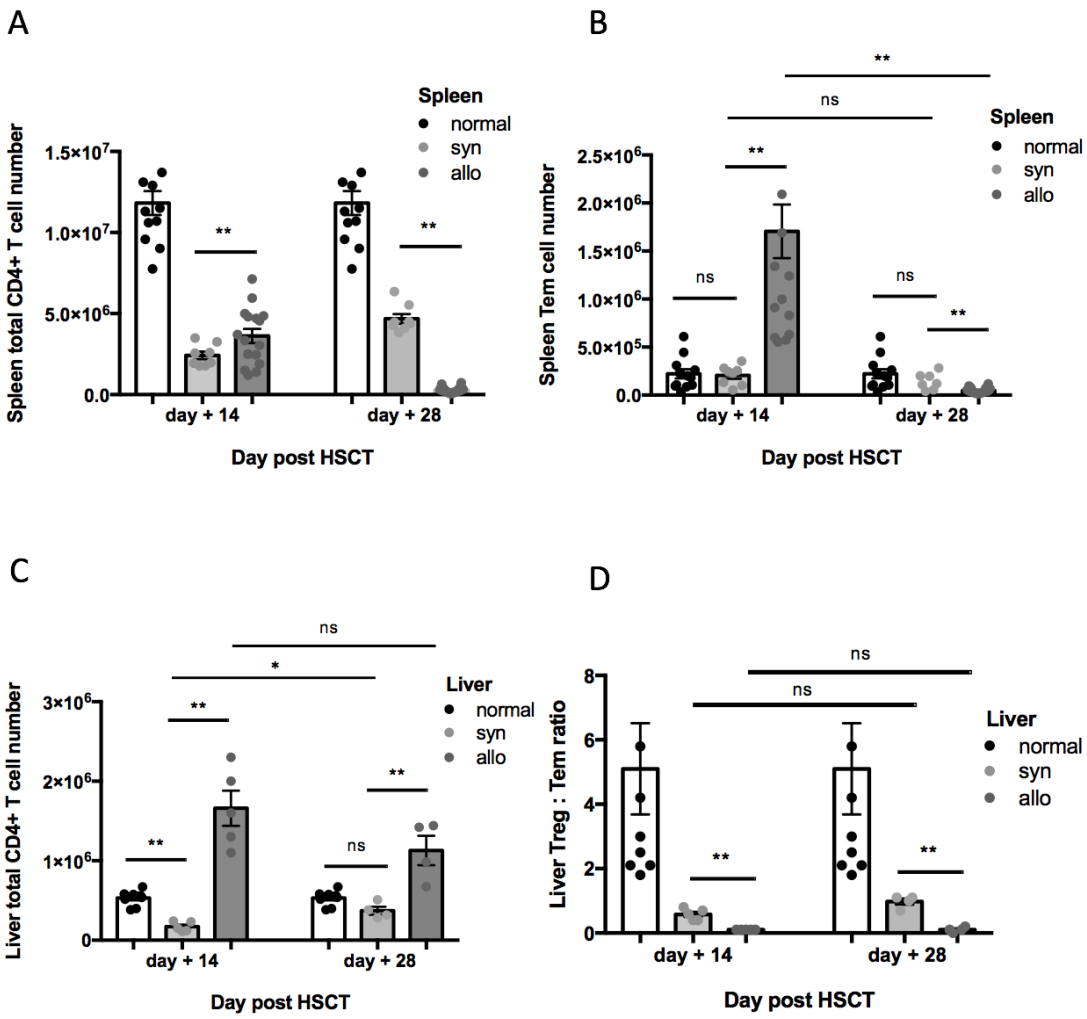

Supplemental Figure 3. Spleen and parenchymal liver CD4+ T cell number and composition for normal mice, syngeneic (syn), and allogeneic (allo) hematopoietic stem cell transplant (HSCT) recipients. (A) The mean spleen total $CD4^+$ T cell number for syngeneic day +14 = 1.7 x 10^6 (n=8), syngeneic day +28 = 4.1 x 10^6 (n=8), allogeneic day +14 = 2.9 x 10^6 (n=16), allogeneic day +28 = 0.2 x 10^6 (n=26), normal = 10.9 x 10^6 (n=12) **(B)** The mean spleen T_{EM} cell number in allogeneic versus syngeneic recipients measured at day +14 and +28. Data for four independent experiments were pooled for these analyses (n = 2 to 7 mice per cohort per time point) and are representative of more than ten independent experiments [**P < 0.01]; Tukey's test with ANOVA. **(C)** The mean liver total $CD4^+$ T cell number for syngeneic day +14 = 0.2 x 10^6 (n=5), syngeneic day +28 = 0.4 x 10^6 (n=8), allogeneic day +14 = 1.7 x 10^6 (n=5), allogeneic day +28 = 1.1 x 10^6 (n=5), normal = 0.5 x 10^6 (n=9); [*P < 0.05, **P < 0.01]; Tukey's test with ANOVA. **(D)** Liver T_{Reg} : T_{EM} ratio is consistently lower in the allogeneic setting compared to that of syngeneic and normal cohorts. Data for two independent experiments were pooled for this analysis (n = 5 to 8 mice per cohort per time point), and are representative of three independent experiments for day +14 [*P < 0.05, **P < 0.01]; Tukey's test with ANOVA.

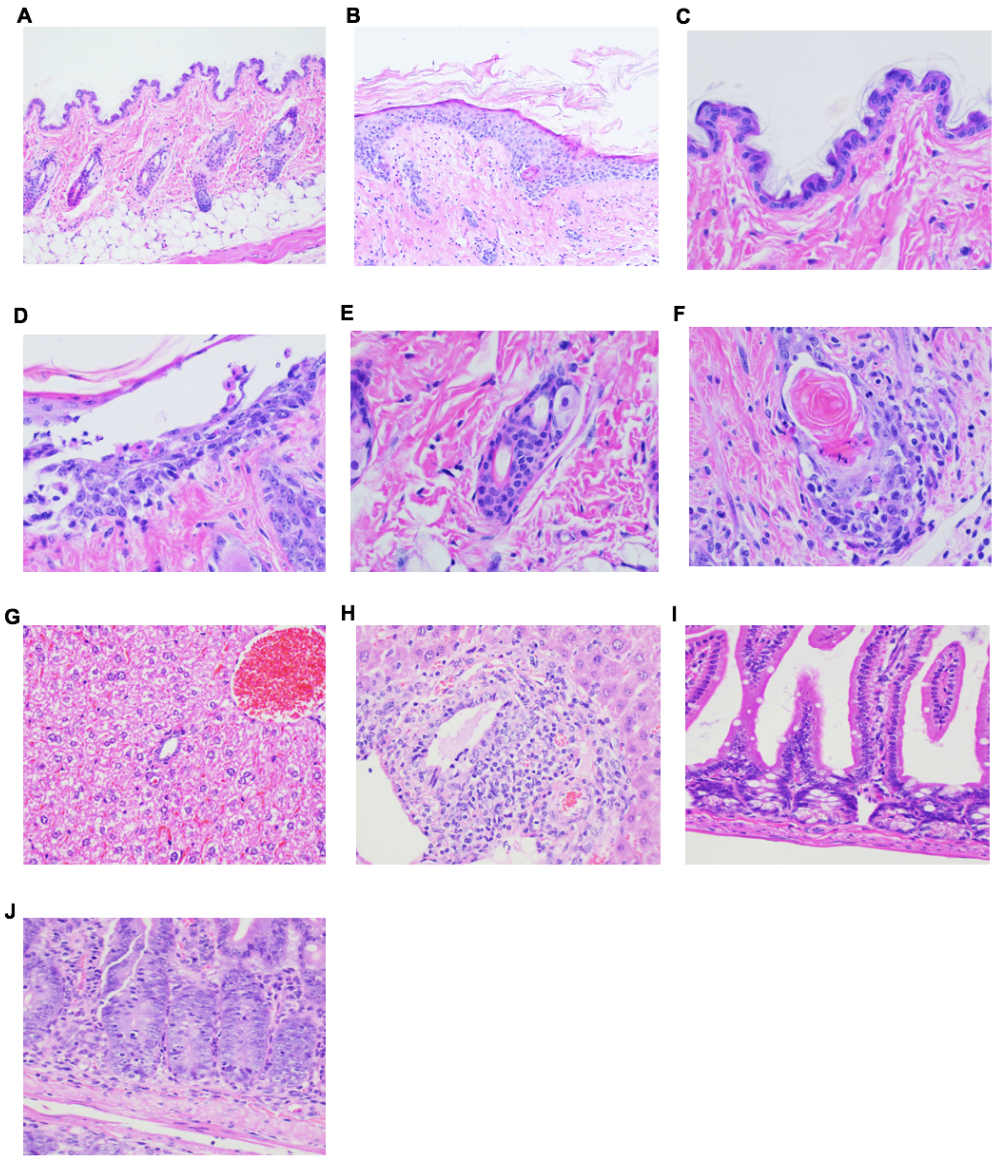

Supplemental Figure 4. Mouse target organ histology and flow cytometry characteristics for syngeneic and allogeneic hematopoietic stem cell transplant (HSCT) recipients. Target organ histology for syngeneic and allogeneic recipients. **(A)** Representative syngeneic HSCT recipient skin section, 200X; normal skin histology is observed at day +14 and day +28. **(B)** Allogeneic HSCT recipient skin section, 200X, day +28. Prominent hyperkeratosis and acanthosis are observed. While the magnification and orientation of the section are similar for **(A)** and **(B)**, in **(B)** hyperkeratosis precludes visualization of additional skin layers (subcutis and muscularis not visualized). **(C)** Syngeneic skin epithelial section, 600X; normal histological appearance. **(D)** Allogeneic skin epithelial section, 600X, day +28; intraepithelial lymphocytes evident with dyskeratotic epithelial cells. **(E)** Syngeneic skin hair follicle section, 600X; normal histological appearance. **(F)** Allogeneic skin hair follicle section, 600X, day +28; intraepithelial peri-follicular lymphocytes and dyskeratotic epithelial cells are evident. **(G)** Syngeneic liver section, 400X, day +14; normal histologic appearance. **(H)** Allogeneic liver section, 400X, day +14; moderate lymphocytic periductal infiltrate is present. **(I)** Syngeneic small intestine section, 400X, day +14; normal intestinal crypt and villi histology is observed. **(J)** Allogeneic section, 400X, day +14; crypt hyperplasia, increased number of epithelial cells, and a lymphocytic infiltrate are observed. Histology findings are representative of two independent experiments (n = 5 mice per cohort per time point).

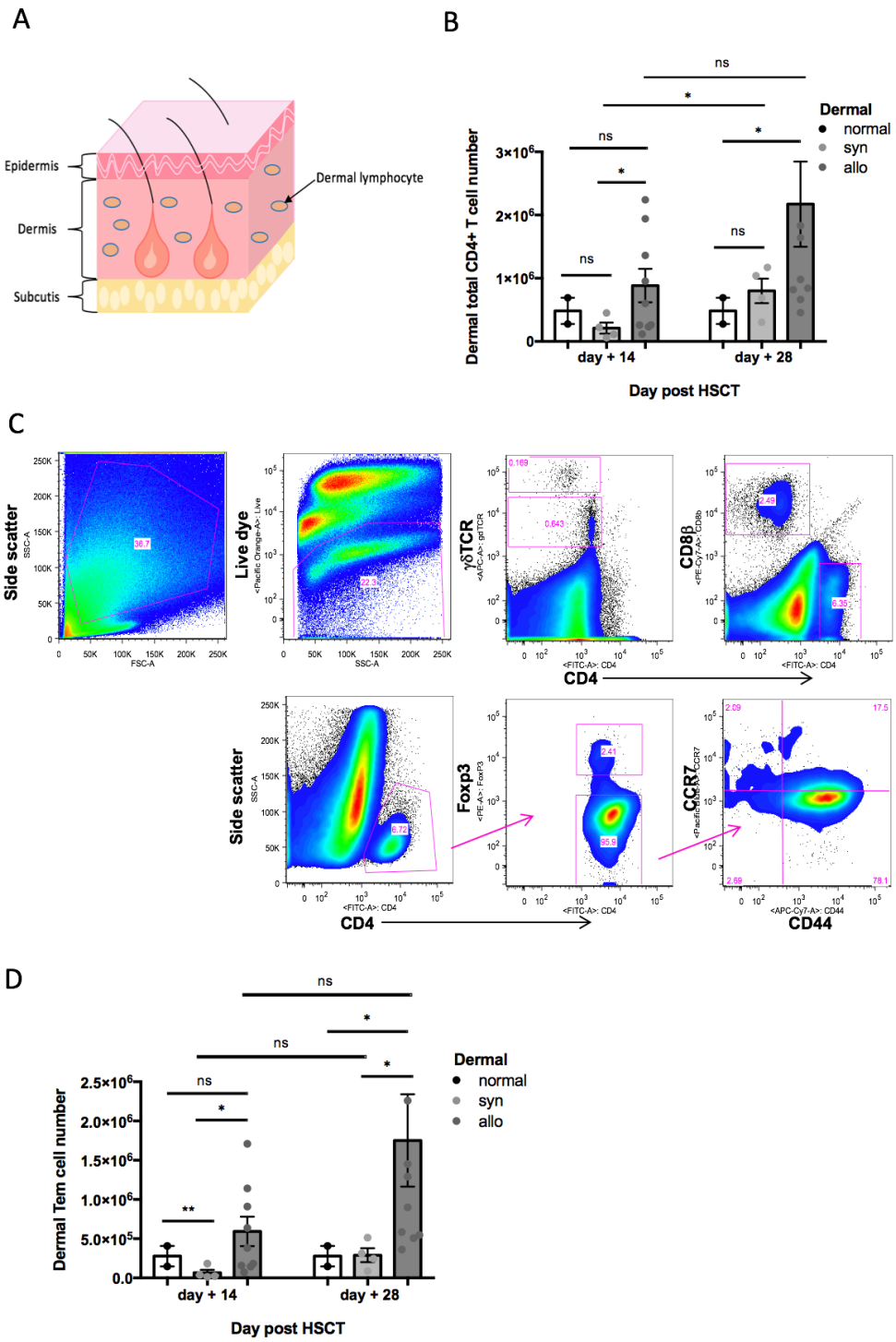

Supplemental Figure 5. Dermal T cell number and composition for normal mice, syngeneic (syn) and allogeneic (allo) hematopoietic stem cell transplant (HSCT) recipients. **(A)** Graphic representation of the different layers of the skin, highlighting the location of dermal lymphocytes. **(B)** The average total number of dermal CD4+ T cells for syngeneic day +14 = 0.6 x 10^6 (n=2), syngeneic day +28 = 1.6 x 10^6 (n=2), allogeneic day +14 = 1.5 x 10^6 (n=4), allogeneic day +28 = 3.7 x 10^6 (n=5), normal = 2.4 x 10^6 (n=2); [*P < 0.05]; Tukey's test with ANOVA. **(C)** Representative flank dermal flow cytometry data for the allogeneic cohort at day +28. Data for two independent experiments were pooled, and are representative of three independent experiments. **(D)** Dermal $CD4^+$ T_{EM} cell number for each experimental cohort measured at day +14 and +28 [*P < 0.05; ** P < 0.01]; Tukey's test with ANOVA.

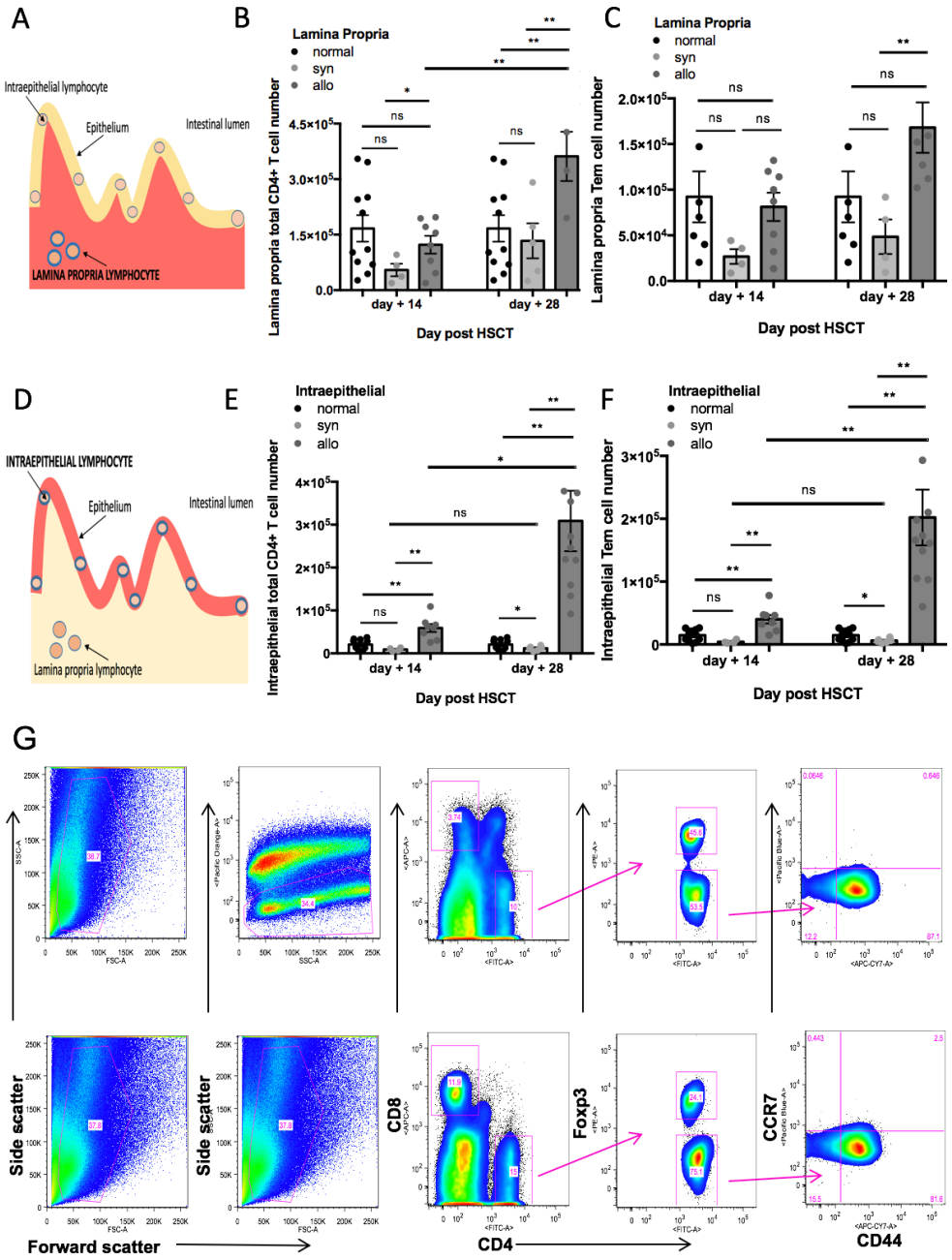

Supplemental Figure 6. Small intestine lamina propria (LP) and intraepithelial (IE) T cell number and composition for normal mice, syngeneic (syn) and allogeneic (allo) hematopoietic stem cell transplant (HSCT) recipients. **(A)** Graphic representation of the different layers of the small intestine, highlighting the location of lamina propria lymphocytes **(B)** Total number of small intestine LP $CD4^+$ T cells for each experimental cohort measured at day +14 (n= 4 for syn, n=8 for allo) and +28 (n=4 for syn, n=7 for allo) (n= 8 for norm). **(C)** Total number of small intestine LP $CD4^+$ T_{EM} cells for each experimental cohort measured at day +14 (n=4 for syn, n=8 for allo) and +28 (n=4 for syn, n=7 for allo) (n= 7 for norm). **(D)** Graphic representation of the different layers of the small intestine, highlighting the location of intraepithelial lymphocytes. **(E)** Total number of small intestine IE $CD4^+$ T cells for each experimental cohort measured at day +14 (n=4 for syn, n=8 for allo) and +28 (n=6 for syn, n=11 for allo) (n= 10 for norm). **(F)** Total number of small intestine IE $CD4^+$ T_{EM} cells for each experimental cohort measured at day +14 (n=4 for syn, n=8 for allo) and +28 (n=6 for syn, n=11 for allo) (n= 10 for norm). **(G)** Flow cytometry gating strategy for small intestine LP samples is displayed, with the upper panels representative of syngeneic data for day +14, and the lower panels representative of allogeneic cohort data for day +14. For panels **(B), (C), (E)** and **(F)**, $*P < 0.05$, $**P < 0.01$; Tukey's test with ANOVA.

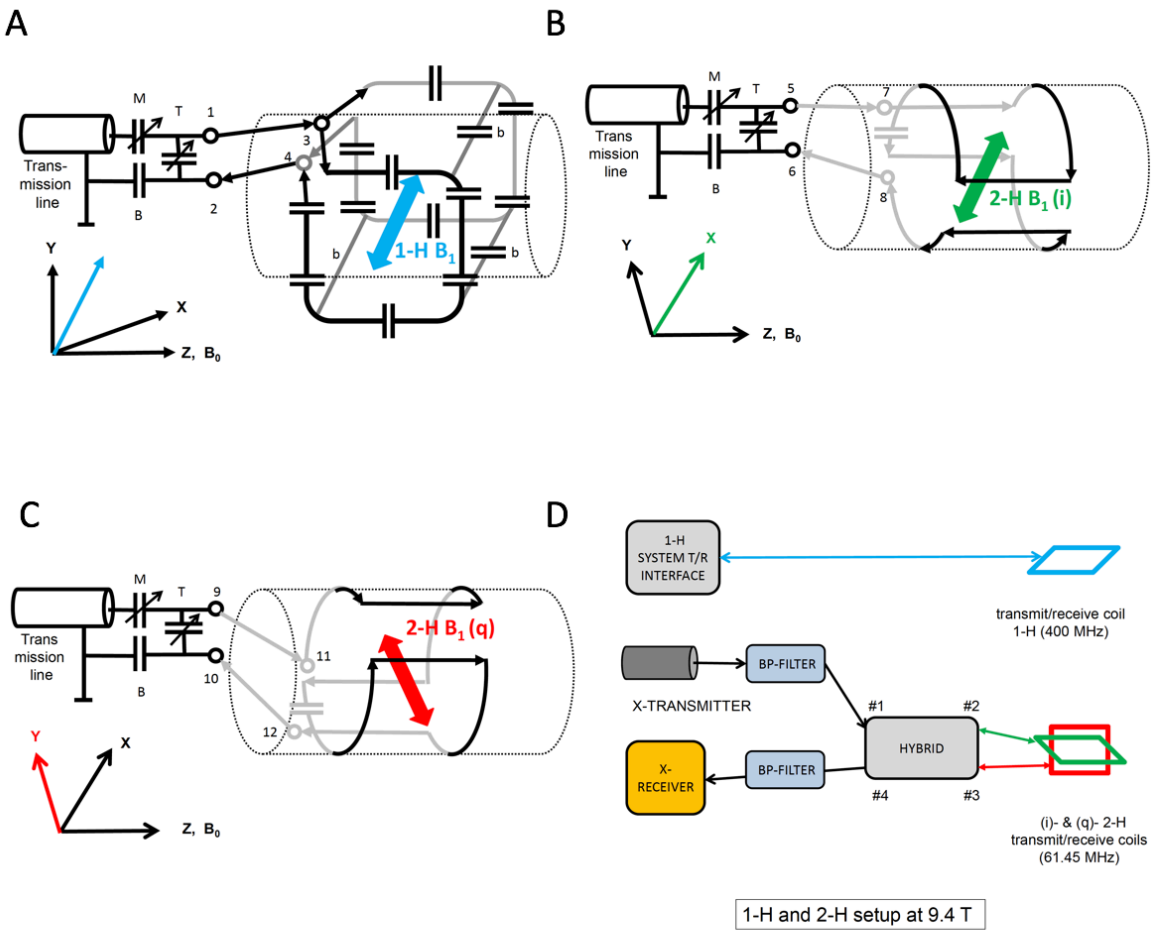

Supplemental Figure 7. Components of the (^{1}H-^{2}H) proton-deuterium coil. **(A)** Schematic of the "quasi Helmholtz" ^{1}H transmit/receive coil for scout (anatomical) imaging. The blue double arrow indicates the B_1 direction in regard to the magnet Cartesian coordinates (B_0=Z=horizontal). **(B)** Schematic of the (q)-channel of the "quasi Helmholtz" saddle-type ^{2}H transmit/receive coil for chemical shift imaging (CSI). The red double arrow indicates the B_1 direction in regard to the magnet Cartesian coordinates (B_0=Z=horizontal). **(C)** Schematic of the (i)-channel of the "quasi Helmholtz" saddle-type ^{2}H transmit/receive coil for CSI. The green double arrow indicates the B_1 direction in regard to the magnet Cartesian coordinates (B_0=Z=horizontal). **(D)** Schematic of the setup for ^{1}H and ^{2}H imaging at 9.4 Tesla magnetic flux density. All coils are mounted on a cylindrical former. The coil described in **(A)**, shown here as a blue circle, is connected in a standard way to the MR system, including the transmit/receive switch. The deuterium coil consists of two identical dual saddle-shaped "quasi Helmholtz" pairs at a 90° angle, described in **(B)** and **(C)** and shown here as red and green circles, respectively. The orthogonal arrangement and 90° phase delayed feeding of the RF current reduces the power requirement for a well-defined flip angle to ½, compared to that needed for a single-saddle coil. In addition, the signal-to-noise ratio is increased by a factor of $\sqrt{2}$. A power transmitter at ^{2}H frequency is connected at port #1 of the hybrid via a bandpass filter to a quadrature hybrid for power splitting and phase creating. Ports #2 and #3 of the hybrid are connected to the two ^{2}H coil ports using identical length cables. The combined signal is received at port #4 of the hybrid that acts as a transmit/receive switch. The signal is passed to another bandpass filter to the x-receive port.